

Article

Electrochemical Sensing and Removal of Cesium from Water Using Prussian Blue Nanoparticle-Modified Screen-Printed Electrodes

Prem. C. Pandey ^{1,*} , Hari Prakash Yadav ¹, Shubhangi Shukla ¹  and Roger J. Narayan ^{2,*} 

¹ Department of Chemistry, Indian Institute of Technology (BHU), Varanasi 221005, India; hariprakashyadav.rs.chy19@itbhu.ac.in (H.P.Y.); shubhangi.rs.chy14@itbhu.ac.in (S.S.)

² Joint Department of Biomedical Engineering, University of North Carolina, Chapel Hill, NC 27599, USA

* Correspondence: pcpandey.apc@iitbhu.ac.in (P.C.P.); rjnaraya@ncsu.edu (R.J.N.)

Abstract: Selective screening followed by the sensing of cesium radionuclides from contaminated water is a challenging technical issue. In this study, the adsorption functionality of Prussian blue (PB) nanoparticles was utilized for the detection and efficient removal of cesium cations. An efficient PB nanoparticle-modified screen-printed electrode (SPE) in the three-electrode configuration was developed for the electrochemical sensing and removal of Cs⁺. PB nanoparticles inks were obtained using a facile two-step process that was previously described as suitable for dispensing over freshly prepared screen-printed electrodes. The PB nanoparticle-modified SPE induced a cesium adsorption-dependent chronoamperometric signal based on ion exchange as a function of cesium concentration. This ion exchange, which is reversible and rapid, is associated with electron transfer in the PB nanoparticle-modified SPE. Using this electrochemical adsorption system (EAS) based on chronoamperometry, the maximum adsorption capacity (Q_{\max}) of Cs⁺ ions in the PB nanoparticle-modified SPE reached up to $325 \pm 1 \text{ mg} \cdot \text{g}^{-1}$ in a $50 \pm 0.5 \text{ } \mu\text{M}$ Cs⁺ solution, with a distribution coefficient (K_d) of $580 \pm 5 \text{ L} \cdot \text{g}^{-1}$ for Cs⁺ removal. The cesium concentration-dependent adsorption of PB nanoparticles was also demonstrated by fluorescence spectroscopy based on fluorescence quenching of PB nanoparticles as a function of cesium concentration using a standard fluorophore like fluorescein in a manner analogous to that previously reported for As(III).

Keywords: Prussian blue nanoparticle; screen-printed electrodes; cesium ion decontamination; electrochemical adsorption system; chronoamperometry; voltammetry



Citation: Pandey, P.C.; Yadav, H.P.; Shukla, S.; Narayan, R.J. Electrochemical Sensing and Removal of Cesium from Water Using Prussian Blue Nanoparticle-Modified Screen-Printed Electrodes. *Chemosensors* **2021**, *9*, 253. <https://doi.org/10.3390/chemosensors9090253>

Academic Editors: Jana Drbohlavová and Agnieszka Mech

Received: 6 July 2021

Accepted: 31 August 2021

Published: 7 September 2021

Publisher's Note: MDPI stays neutral with regard to jurisdictional claims in published maps and institutional affiliations.



Copyright: © 2021 by the authors. Licensee MDPI, Basel, Switzerland. This article is an open access article distributed under the terms and conditions of the Creative Commons Attribution (CC BY) license (<https://creativecommons.org/licenses/by/4.0/>).

1. Introduction

The Fukushima Daiichi nuclear disaster was associated with the release of radionuclide-containing water, including 940 TBq of radioactive cesium (¹³⁷Cs), into the sea. The ¹³⁷Cs radionuclide, which exhibits a half-life of 30 years, is hazardous due to the emission of beta-particles and strong gamma rays. Therefore, removing ¹³⁷Cs from contaminated water has become a research issue of growing significance [1,2]. Many adsorbent materials (e.g., clay minerals and metal oxides) have been evaluated in terms of their capability for removing ¹³⁷Cs from contaminated water [1–11]. Many of these conventional adsorbents are too expensive for use in large-scale applications or are too difficult to synthesize. Prussian blue (PB), also called ferric hexacyanoferrate, is a zeolite-like inorganic material that exhibits a face-centered cubic lattice; PB substitutes its potassium ions for cesium ions due to the fact that it shows a high affinity for Cs in solution [3]. Accordingly, many reports on the use of PB and its analogs have demonstrated the removal of cesium ions [4–11]. These reports [4–11] confirmed the active role of PB in cesium adsorption; the removal efficiency of cesium is the function of parameters associated with the properties of PB and the additives that are used to prepare the adsorbent. In addition, PB exhibited well-defined redox electrochemistry associated with two redox couples, PB/PB white (PW)

and PB/berlin green (BG), which may be explored for simultaneous sensing of cesium ions during adsorption dynamics. The approach can involve layering of the PB over the electrodes. Accordingly, this study involved understanding the electrochemical adsorption and sensing behavior of a PB-modified electrode. It has been previously shown that PB serves as an artificial peroxidase and displays electrochemical behavior as a function of hydrogen peroxide concentration [12–16]. In addition, recent studies indicate that PB can be used for the sensing and screening of As(III) in water [15], which directed us to examine the selectivity, if any, on the interaction dynamics of PB and appropriate analytes (hydrogen peroxide, arsenic (III) ions, and cesium ions) using PB-modified electrodes.

The unique ability of PB to adsorb hydrated Cs^+ is attributed to its regular lattice spaces that are encircled by cyanide-bridged metals and proton exchange. The adsorption functionality of PB for alkali metal ions increases in the following manner: $\text{Cs}^+ \gg \text{K}^+ \geq \text{Na}^+$. Although PB has excellent potential use for adsorbent applications, PB nanoparticles are prepared as a very fine powder by the precipitation approach. Due to its long sedimentation time, it is difficult to separate PB from an aqueous solution via filtration or centrifugation, necessitating the use of a costly membrane for filtration after Cs adsorption. In addition, nano-sized particles also often form agglomerations to minimize their surface energy.

The controlled synthesis of PB and its mixed metal analogs has been previously evaluated; the processability and nanoscale geometry of this material have been demonstrated [12–16]. It should be noted that PB is a US Food and Drug Administration-approved drug for the treatment of radioactive exposure and has been clinically used for the treatment of ^{137}Cs -contaminated individuals [17]. However, the use of PB for water treatment is not an efficient process since the isolation of Cs-loaded PB from water is both time-consuming and costly. Therefore, a “green” and economical technique for both PB immobilization and separation would be of significant benefit, specifically the development of a PB-based formulation that can be converted into a homogeneous colloidal solution or embedded within a heterogeneous matrix that is suitable for the removal of Cs.

The process of Cs removal also involves monitoring the presence of Cs in a given sample before and after Cs treatment. Electrochemical sensors have recently been described for the detection and removal of Cs [18]. However, the use of conventional electrodes [18] for PB nanoparticle-modified electrodes exhibits major disadvantages, including (1) poor control over the PB film on the electrode surface, and (2) a bulky structure that is associated with poor cesium adsorption efficiency. The use of screen-printed electrodes (SPEs) [19–22] has been demonstrated successfully in several applications over the past 3 decades. In addition, SPEs are preferable over conventional electrodes since they can be made in several geometries, including in multiplexed formats, out of a variety of materials; in addition, SPEs can be produced in large quantities at low cost. Furthermore, SPEs provide reproducible surfaces [19–22], which are needed to obtain repeatable electrochemical data. In addition, electrodes in the three-electrode configuration can be inexpensively printed with graphite paste and Ag/AgCl paste using commercial screen-printing technology, followed by precise layering of active PB nanoparticle ink over the working electrode. Since the redox electrochemistry of PB is related to the number of deposited PB layers on the screen-printed electrode, dispensing of PB ink to create a PB film over the screen-printed electrode was performed in order to enhance the PB adsorption efficiency and sensing functionalities. We have recently described screen-printed electrodes that are commercially available [<http://www.sensors-vns.com> (accessed on 31 December 2003), <https://www.sensors-vns-opc.com> (accessed on 31 December 2019)]; the functionality of these SPEs for Cs detection is reported in this study.

2. Experimental Section

2.1. Materials

Sodium arsenite was purchased from S D Fine-chem Limited (Mumbai, Maharashtra, India). Cesium chloride, tetrahydrofuran, and hydrogen peroxide were purchased from Sisco Research Laboratories Pvt. Ltd. (Mumbai, Maharashtra, India). Potassium

ferricyanide was obtained from MilliporeSigma India (Bengaluru, Karnataka, India). The remaining chemicals were purchased from commercial sources and were of analytical grade. Milli-Q water was used throughout the experiment to avoid interference from contaminants.

2.2. Synthesis of PB Nanoparticle Ink

The PB nanoparticle ink needs to be dispensed and cured under appropriate conditions that enable the PB character of the ink to be retained; the suitable binder and the viscosity of the PB formulation are important parameters. The following approach has been adopted for dispensing PB ink over the working electrode surface of SPEs, followed by straightforward curing for electrochemical measurements.

Hydrogen Peroxide and Tetrahydrofuran-Mediated Synthesis of PB Nanoparticles

The synthesis of a PB nanoparticle colloidal suspension was accomplished according to a procedure described earlier [16] using tetrahydrofuran and hydrogen peroxide from the single precursor potassium ferricyanide via chemical reduction. The homogeneous colloidal sol of PB nanoparticles was prepared by adding 20 μL of tetrahydrofuran (0.1 M) and 50 μL of hydrogen peroxide (0.5 M) to 100 μL of potassium ferricyanide (0.03 M) under stirring conditions; this mixture was kept in an oven at 343 K for 6 h.

2.3. Fabrication of PB Nanoparticle-Modified Screen-Printed Electrodes

Screen-printed electrodes (SPE) in the 3-electrode configuration as shown in Figure 1 were developed using silver, graphite, and Ag/AgCl pastes as shown below via screen printing technology; graphite was used for the working and counter electrodes; Ag/AgCl was used for the reference electrode. The working electrode track of the freshly prepared SPE was further modified with a Nordson dispenser using PB nanoparticle printing ink and dried at 380 K for 1 h.

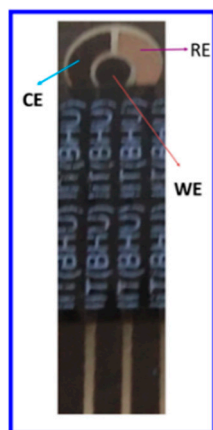


Figure 1. Homemade screen-printed electrode (WE = working electrode, RE = reference electrode and CE = counter electrode).

2.4. Electrochemical Measurements

Electrochemical studies (e.g., differential pulse voltammetry, cyclic voltammetry, chronoamperometry, and electrochemical impedance spectroscopy (EIS)) were performed with a PB nanoparticle-modified SPE in a 3-electrode configuration using a CHI Instruments Electrochemical Workstation Model 660 (Austin, TX, USA) with a working volume of 3 mL and a specially designed electrochemical cell that was equipped with electrode holder for SPE. A PB nanoparticle-modified electrode (GCE) was used as the working electrode. The electrochemical cell was degassed through purging with nitrogen gas when necessary.

2.5. Assessment of Electrochemical Adsorption

The electrochemical adsorption (EA) was evaluated in 1 ppm Cs⁺ solution at 0.25 V under stirring using chronoamperometry. For chemical adsorption (CA), procedures similar to the EA method without potential were undertaken. After adsorption, the Cs⁺ ions in solution were measured by ICP-MS. The Cs⁺ removal performance was calculated using removal efficiency (R%) and uptake capacity (Q_e) values as follows [17,18,23]:

$$R\% = \frac{(C_0 - C_e) \times 100}{C_0}$$

$$Q_e(\text{mg/g}) = \frac{(C_0 - C_e) \times V}{M}$$

In this equation, C₀ and C_e are the initial concentrations of the cesium ions before adsorption and after adsorption at the equilibrium state, respectively, V is the volume of the solution, and M is the mass of the adsorbent.

The mechanism of electrochemical adsorption mode was identified following both single and multilayer adsorption curves using the Langmuir and Freundlich adsorption isotherm, respectively; the relevant equations are given below:

$$Q_e = \frac{Q_{\max} \times K_L \times C_e}{1 + K_L C_e} \text{ for Langmuir adsorption isotherm}$$

$$Q_e = K_F C_e^{1/n} \text{ for the Freundlich adsorption isotherm}$$

In this equation, Q_{max} (mg·g⁻¹) is the maximum adsorption capacity, K_F (L·mg⁻¹) is Freundlich constant related to adsorption capacity, K_L (L·mg⁻¹) is the Langmuir constant related to the free energy of adsorption, and n is the Freundlich exponent.

The selectivity for Cs⁺ is determined from the distribution coefficient (K_d) using the expression below [18]:

$$K_d(\text{mg/g}) = \frac{(C_0 - C_t) \times V}{C_0 \times M}$$

The K_d value was obtained using EA or CA system in the presence of 1 mM interfering alkali ions containing 1 ppm Cs⁺ ions. The Cs⁺ ions in solution were monitored by ICP-MS.

2.6. Fluorometric Method

A fluorometric method was utilized to understand cesium-mediated fluorescence quenching; the obtained values were compared to those recorded for As(III) as reported earlier [15]. Fluorescein was used as probe molecule (λ_{ex} = 480 nm, λ_{em} = 510 nm). The fluorescence experiment was performed using neutral pH (6.8) with Milli-Q water. Different concentrations of cesium chloride standard solution (10 ppm to 500 ppm) were prepared by adding appropriate amounts of cesium chloride to Milli-Q water. The result was determined with the effective concentration of PB nanoparticles, fluorescein, and Cs⁺.

3. Results and Discussion

3.1. Tetrahydrofuran and H₂O₂-Mediated Synthesis of PB Nanoparticle Ink and Electrochemical Performance of PB Nanoparticle-Modified Screen-Printed Electrode

The conventional synthesis of PB is followed by agglomeration of nuclei into large particles; this phenomenon is associated with the poor processability of PB into PB film-modified electrodes [13,14]. Accordingly, we have demonstrated an efficient approach that enables the controlled conversion of the single precursor potassium ferricyanide into PB nanoparticles as shown in TEM images (Figure 2) using small organic reducing agents [13–16]. We have already demonstrated that the organic reagent tetrahydrofuran in the presence of hydrogen peroxide enabled the conversion of K₃[Fe(CN)₆] into PB nanoparticles [16]. The as-made nanoparticles were readily converted into a screen printable ink of appropriate viscosity by high-speed centrifugation at 50,000 rpm, which enabled

straightforward removal of the lighter components of the PB nanoparticle suspension to the desired viscous PB nanoparticle suspension. The SEM images, EDX data, and UV-VIS spectra showing the formation of PB nanoparticles are shown in Figure 3. The suspension of as-made PB was dispensed easily onto the working portion of the SPE using a Nordson Dispenser and was cured at a temperature of 383 K between 20 min and 1 h.

We recently demonstrated that PB nanoparticles served as an efficient nanomaterial for sensing and removal of As(III) [15]. In order to understand the utility of PB for sensing and removal of cesium ions, it is important to discriminate the interaction of PB with hydrogen peroxide, arsenic (III), and cesium ions. Since PB nanoparticles are a well-known peroxidase mimetic, PB nanoparticle-modified screen-printed electrodes undergo selective reduction of hydrogen peroxide close to 0.2 V vs. Ag/AgCl. Recent work [15] indicated that the variation in peak current as a function of hydrogen peroxide and arsenic (III) concentrations occurred in opposite directions, revealing the introduction of selective electrochemical sensing of these 2 analytes. Accordingly, there was an attempt to evaluate the electrochemical sensing of cesium ions under similar conditions was undertaken in order to understand the electrochemical behavior of the PB-modified electrode in the presence of these analytes.

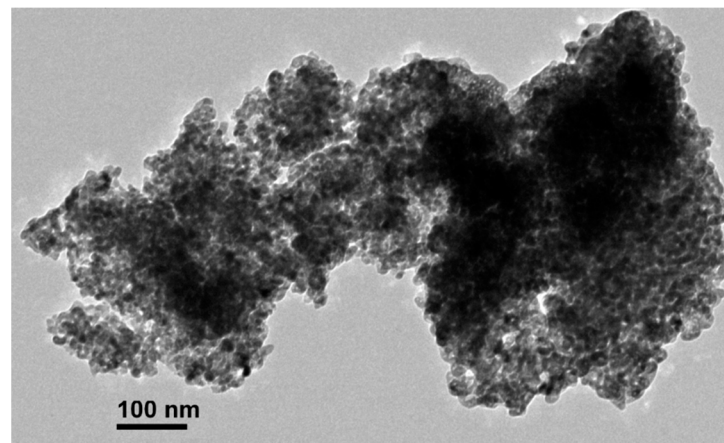
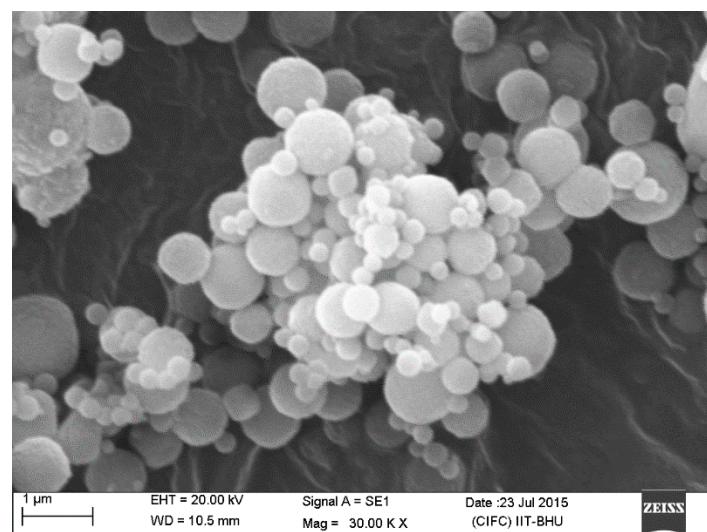


Figure 2. TEM image of PB nanoparticles.



(a)

Figure 3. Cont.

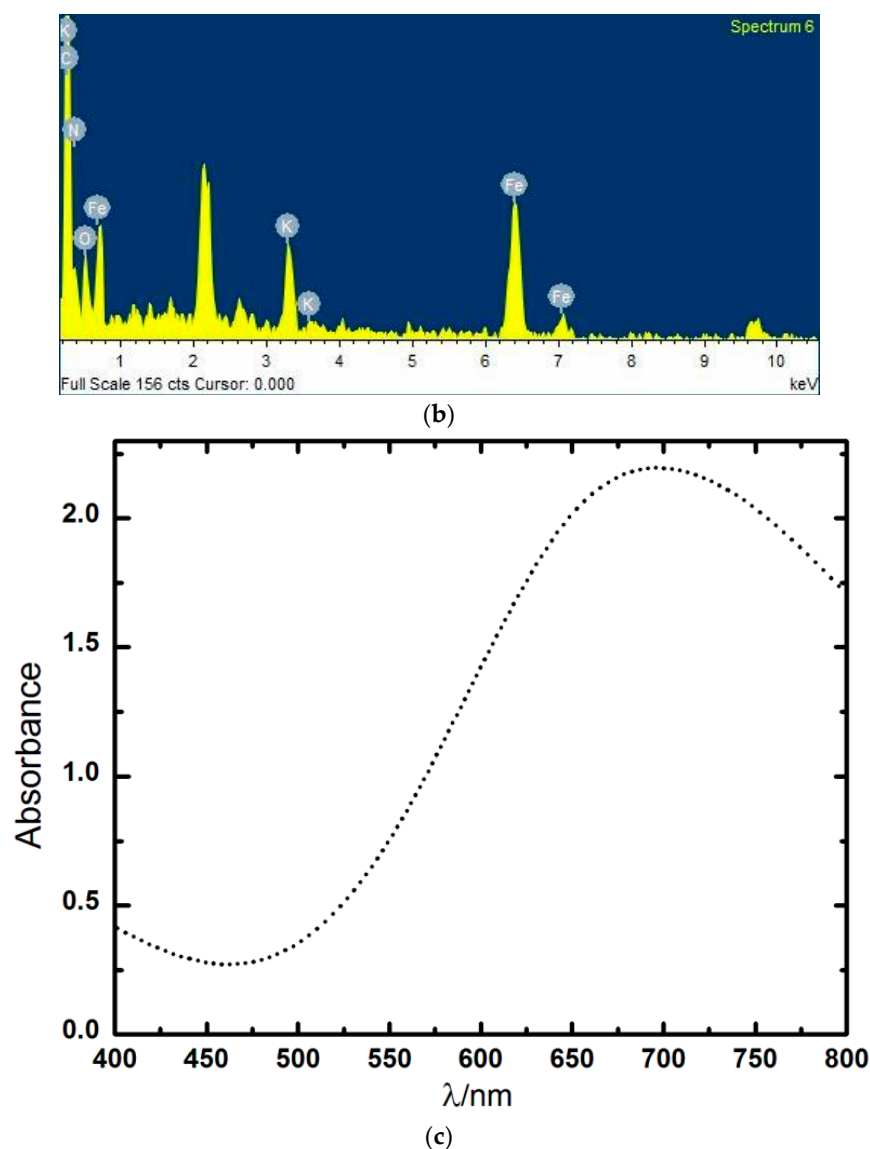


Figure 3. (a) SEM image of PB nanoparticles. (b) EDX of PB nanoparticles. (c) UV-VIS spectra of PB nanoparticles.

3.2. Electrochemistry of PB Nanoparticle-Modified SPE in the Presence of As(III) and Hydrogen Peroxide

The electrochemistry of the PB nanoparticle-modified SPE in the presence of As(III) and H_2O_2 was examined using differential pulse voltammetry (Figure 4) and electrochemical impedance spectroscopy (EIS) as shown in Figure 5. In order to understand the dependence of the peak current of DPV on the analyte concentration, we first examined the variation of the peak current in the presence of H_2O_2 since PB nanoparticles act as a potent peroxidase mimetic and enable selective reduction of the same at the PB nanoparticle-modified electrode close to 0.2 V vs. Ag/AgCl. The results from differential pulse voltammetry are shown in Figure 4A in the absence and the presence of different concentrations of hydrogen peroxide between 0 and 10 mM. The peak current tended to increase with a rising concentration of hydrogen peroxide, indicating a PB nanoparticle-mediated reduction of the same with the electrochemical transition of the $\text{Fe}^{2+}/\text{Fe}^{3+}$ couple. The increase in peak current was concurrently justified with an increase in Fe^{3+} as a function of hydrogen peroxide concentration. Subsequently, we examined the variation in the peak current of DPV under similar conditions as a function of the As(III) concentration as shown in Figure 4B. The following results were noted: (1) the peak current displayed a

pH-dependent behavior, with relatively better variation in the peak current at a pH of 9.0 in the presence of As (III), and (2) the peak current tended to decrease with an increase in the concentration of As (III); the opposite trend was recorded in the presence of hydrogen peroxide. An increase in Fe^{2+} as a function of As (III) concentration was recorded, suggesting the oxidation of As (III) into As (V). These findings clearly predict an analyte-dependent intervalence transition between Fe^{2+} and Fe^{3+} . In order to gain a better understanding of the electrochemical interface, we have further characterized the performance of the PB nanoparticle-modified electrode by electrochemical impedance spectroscopy.

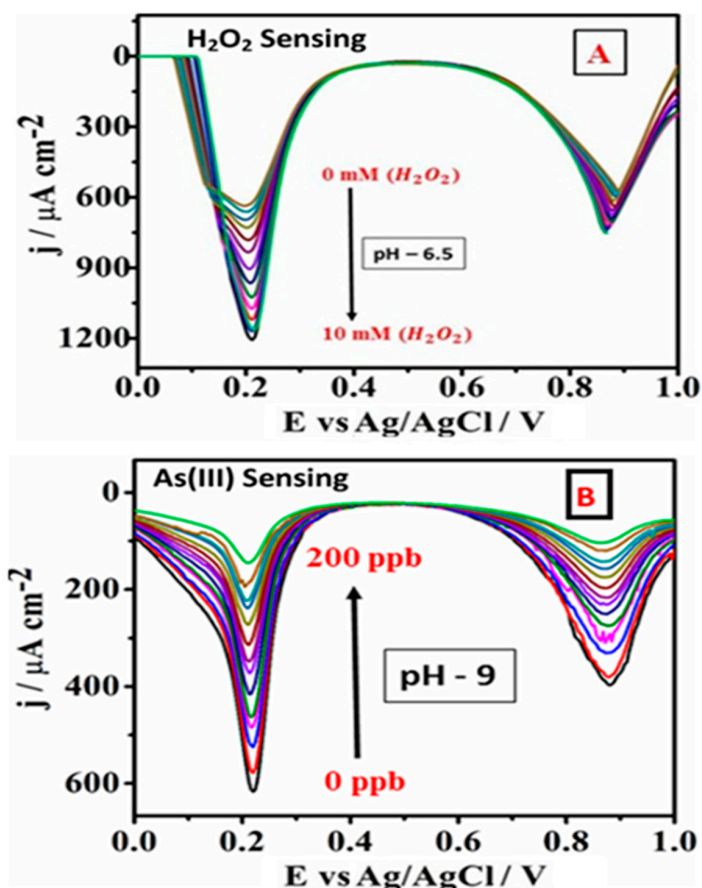


Figure 4. Differential pulse voltammetry of the PB nanoparticle-modified screen-printed electrode in the presence of varying concentrations of hydrogen peroxide. (A) (mM): 0.063, 0.126, 0.25, 0.4, 0.8, 1, 2, 3, 4, 5, 8, 10, and As (III). (B) (ppb): 20, 40, 60, 80, 100, 120, 140, 160, 180, 200.

The electrochemical impedance spectroscopy of the PB nanoparticle-modified electrode is shown in Figure 5 in the absence and the presence of various concentrations of H_2O_2 and As (III). The Nyquist plot in the absence and the presence of H_2O_2 and arsenite is shown in Figure 5A,B, respectively. The impedance spectra shown in Figure 5 include a semicircle portion, corresponding to charge transfer resistance, and a linear portion, corresponding to a diffusion-limited process. EIS of the bare PB nanoparticle-modified electrode (Figure 5) exhibited a nearly straight line; these features indicate the diffusion limiting step of an electrochemical process. In addition, the electron-transfer resistance (R_{et}) corresponds to the semicircle diameter. The semicircle diameter for the PB nanoparticle-modified electrode in the presence of H_2O_2 tended to decrease as compared to that of the PB nanoparticle-modified electrode in the presence of As (III) as shown in Figure 5A,B, respectively. This result indicates a predominantly diffusion limiting step of the electrochemical process between PB nanoparticles and As (III) and electron-transfer resistance in the presence of H_2O_2 ; this result was associated with the analyte-dependent intervalence

transition between Fe^{2+} and Fe^{3+} . The peak current of differential pulse voltammograms in the absence and the presence of As (III) and H_2O_2 was used to construct calibration plots for electrochemical analysis of these analytes. The difference in peak current in the absence of the analyte (I_{pc}) and in the presence of the analyte (As (III)/ H_2O_2) (I_{px}) was used to construct the calibration plot for the analysis of As (III) and H_2O_2 (e.g., $[I_{px}-I_{pc}]$ vs. $\log C$, where C is the concentration of As (III) in ppm (Figure 6A) and H_2O_2 in mM (Figure 6B)). An excellent linear relationship with the lowest detection limit of 0.01 ppb of As (III) justified the use of the PB nanoparticle-mediated electrochemical approach of sensing of As (III); electrochemical oxidation of As (III) as well as the opposite reaction for hydrogen peroxide were demonstrated.

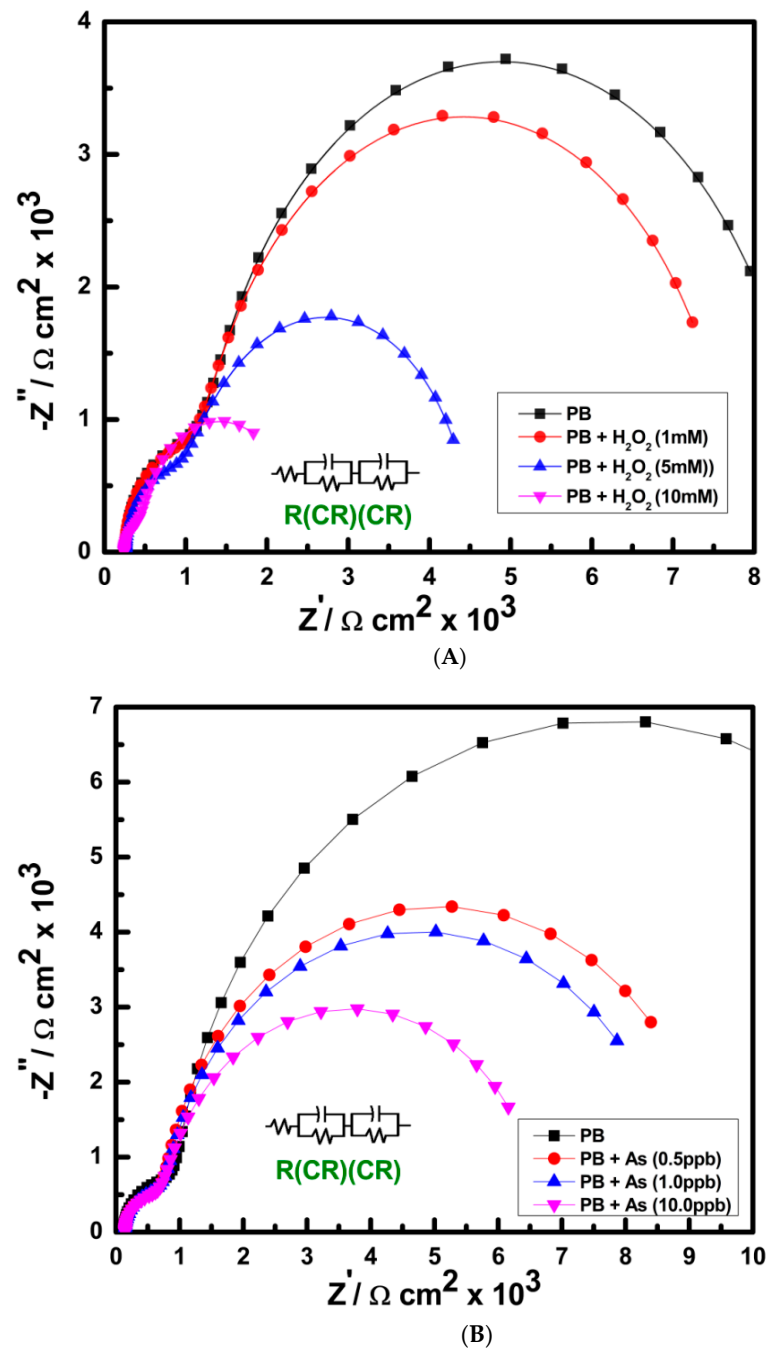


Figure 5. (A). Nyquist plot of the PB nanoparticle-modified electrode in the presence of varying concentrations of hydrogen peroxide. (B). Nyquist plot of the PB nanoparticle-modified electrode in the presence of varying concentrations of As(III).

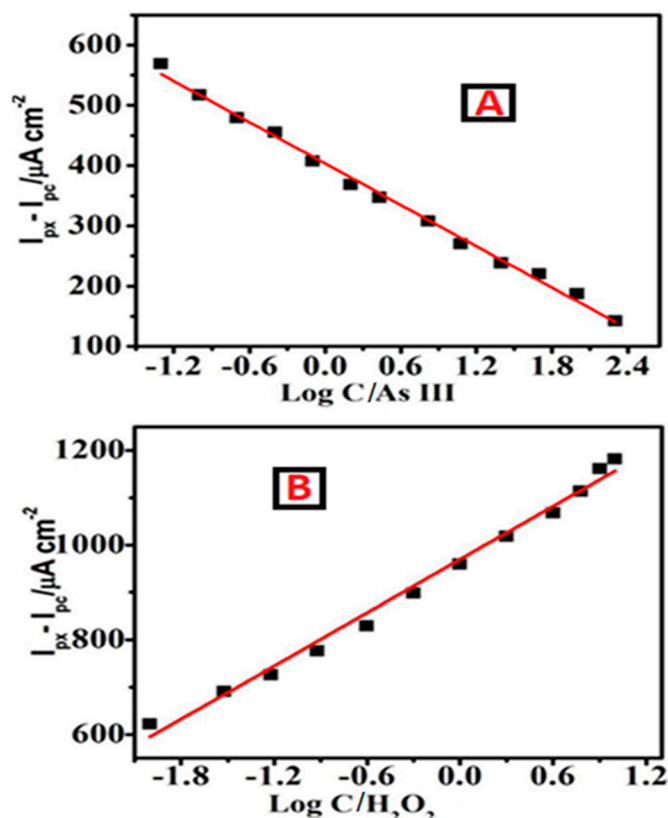


Figure 6. Calibration curve for the analysis of As (III) (A) and hydrogen peroxide (B) based on differential pulse voltammetry.

3.3. Electrochemistry of PB Nanoparticle-Modified Screen-Printed Electrodes in the Presence of Cs Ions

In order to understand the dependence of the electrochemical behavior of the PB nanoparticle-modified SPE as a function of the Cs concentration, we investigated the cyclic voltammogram of the same in the absence and in the presence of Cs ions (Figure 7). The results from the cyclic voltammograms as shown in Figure 7 revealed that the redox peak close to 0.22 V vs. Ag/AgCl did not change significantly, whereas the second redox couple of the PB nanoparticles close to 0.88 V vs. Ag/AgCl showed an increase in anodic current after the addition of 1 mM Cs ions. These results indicated the need to understand the variation of anodic current as a function of the Cs ion concentration based on differential pulse voltammetry. The results as shown in Figure 7 show the differential pulse voltammograms in the presence of varying concentrations of Cs ions.

The results as shown in Figure 8 justify the dependence of the second redox couple of the PB nanoparticles on the cesium concentration; similar results revealed variation of the anodic current of the first redox couple of PB nanoparticles as a function of As(III) and hydrogen peroxide concentrations. This observation indicated the dependence of the electrochemical behavior of PB nanoparticles on the nature of cations and suggested selectivity in the ion exchange electrochemical process. The results shown above indicate that the electrochemical response of the modified electrode was dependent on the analyte. Since cesium ions are associated with concentration-dependent electrochemical behavior that is analogous to that reported for cesium adsorption [15], the adsorption efficiency of the PB nanoparticle-modified SPE was considered.

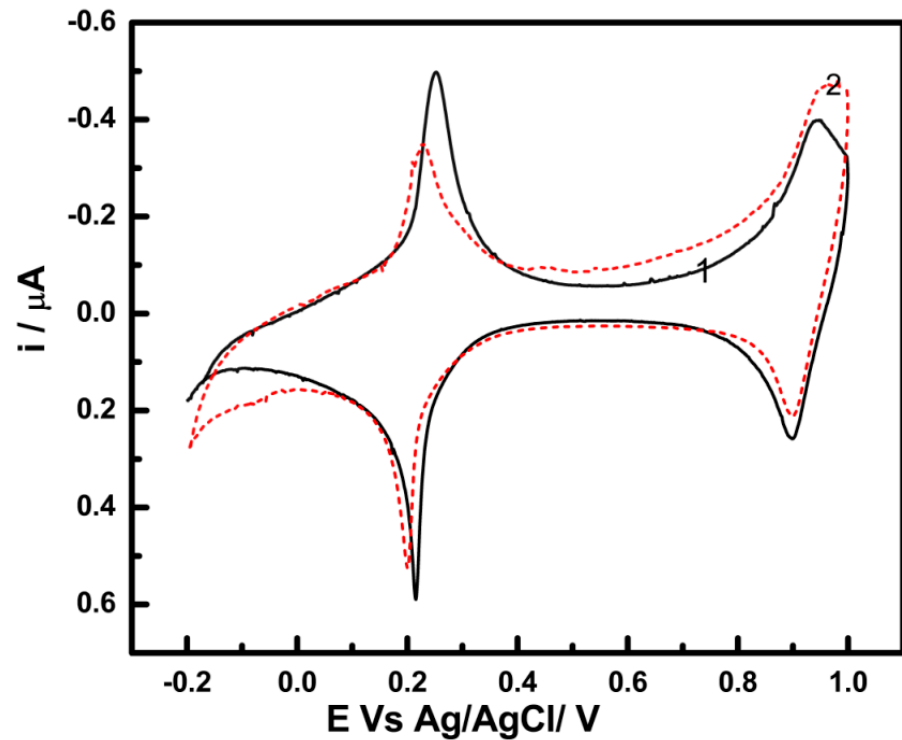


Figure 7. Cyclic voltammogram of the PB nanoparticle-modified screen-printed electrode in 0.1 M KCl at a scan rate of 10 mV/s in the absence (1) and the presence (2) of 1 mM Cs ions.

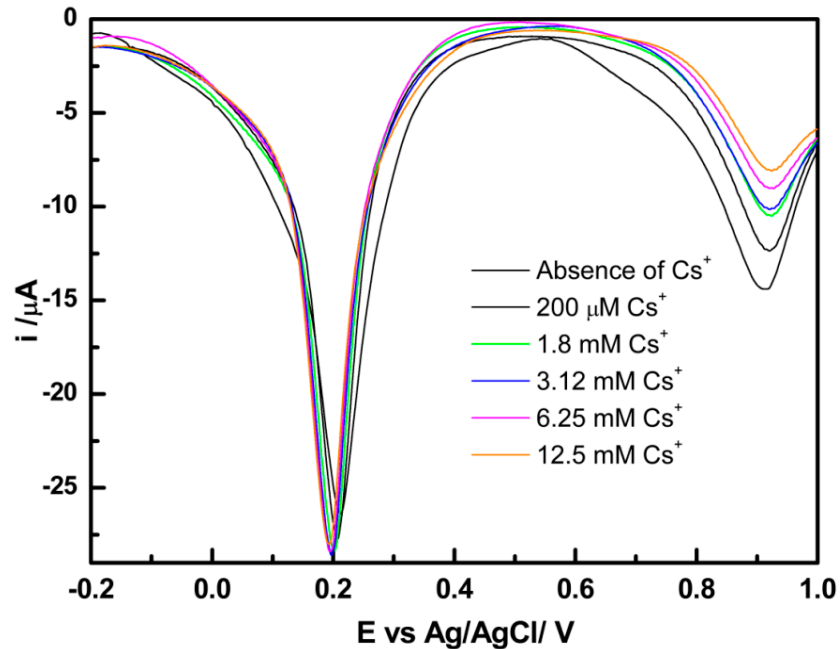


Figure 8. Differential pulse voltammetry of the PB nanoparticle-modified screen-printed electrode in the presence of varying concentrations of Cs ions.

3.4. The Electrochemical Adsorption (EA) Performance of PB Nanoparticle-Modified SPE

The electrochemical adsorption (EA) of Cs⁺ ions was evaluated by chronoamperometry using 1 ppm Cs⁺ solution. Chronoamperometric curves of the PB nanoparticle-modified SPE at various applied potentials in 1 ppm Cs⁺ solution were developed. The cathodic current fell at the initial stage, which reflected the creation of double-layer capacitance; it then approached Cs⁺ adsorption balance at a steady state. Figure 9 shows that Cs⁺ adsorp-

tion showed optimum potential at 0.88 V; at this potential value, Cs⁺ adsorption is driven by a large cathodic current. Use of the EA system for Cs⁺ removal was evaluated using ICP-MS analysis; Q_e and R% data were obtained for the pure PB nanoparticle-modified SPE in 1 ppm Cs⁺ solution with the EA system after 1 h polarization at 0.88 V vs. Ag/AgCl. The removal performance of Cs⁺ ion using the CA system was also investigated for the PB nanoparticle-modified SPE; a larger Q_e of 181 mg·g⁻¹ with 95% Cs⁺ ion removal was obtained using this EA system. The Q_{max} value of the PB nanoparticle-modified SPE for Cs⁺ ions was 325 mg·g⁻¹ when the Cs⁺ ion equilibrium concentration reached up to 50 μM; these adsorption data were in good agreement with the Langmuir isotherm. The K_d value for the PB nanoparticle-modified SPE reached up to 580 L·g⁻¹, indicating efficient performance for cesium removal. Similar procedures are being adopted to make CuHCF-modified SPEs with enhanced performance for cesium removal as reported earlier [18]. A comparison of the adsorption parameters using various forms of adsorbents based on Prussian blue and its analogs is given in Table 1, which indicates the advantage of the PBNP-modified electrode in cesium adsorption.

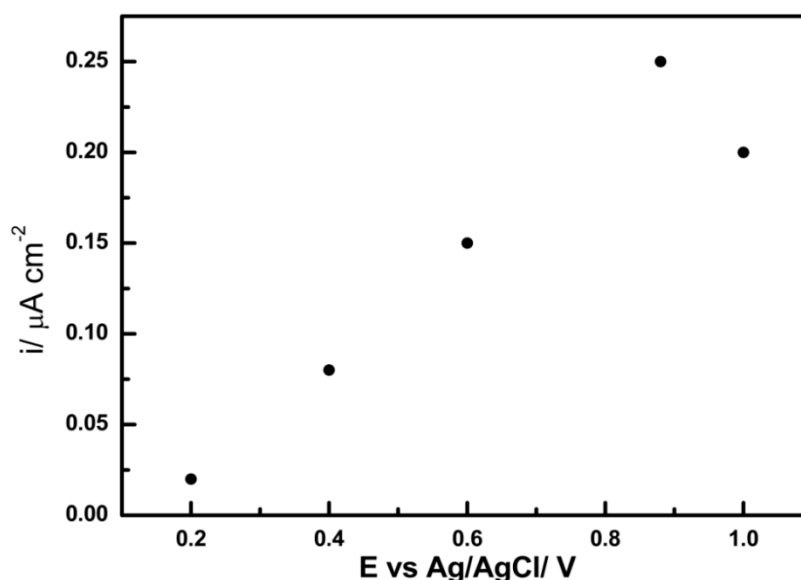


Figure 9. The dependence of chronoamperometric steady current response on the applied potential.

Table 1. Prussian blue (FeFCF) and its analog-based adsorbents for cesium removal.

PB-Based Adsorbent	Removal Efficiency	K _d L/g	Initial Conc. mg/L	Isotherm	Kinetic Model	Q _{max} mg/g	Reference
MWCNT-CuHCF	95	568	1	Langmuir Freundlich	NA	310	[18]
SWCNT-CuHCF	NA	NA	NA	NA	NA	230	[24]
MWCNT-Na-CoHCF-alginate	53	23	200	Langmuir Freundlich	PFO PSO	133	[25]
Fe ₃ O ₄ -FeHCF-GO-alginate beads	80	48.7	25–150	Langmuir Freundlich	PSO	43.5	[26]
Fe ₃ O ₄ -FeHCF-hydrogel	99.5	0.4	100–500	Langmuir	PSO	41.5	[27]
Chitosan-FeHCF-CNT	NA	42.5	1–100	Langmuir Freundlich Redlich Peterson	PFO PSO Webb Morris Elovich	219	[28]
rGO-FeHCF	99.5	6.46	0.2	Langmuir Freundlich	NA	18.67	[29]
FeHCF modified screen-printed electrode	95	580	1	Langmuir Freundlich	NA	325	Present work

3.5. Fluorometric Study

Effect of the Addition of Cs⁺ on the Fluorescent Intensity of Fluorescein

PB nanoparticles have already been demonstrated as light-quenching material; the PB nanoparticle-mediated fluorescence quenching of fluorescein has previously been evaluated for As(III) sensing [15]. Accordingly, we examined how PB nanoparticles behave in the presence of cesium. The impact of As(III) on fluorophore activity was studied earlier [15]; an As (III) concentration-dependent increase in the fluorescence signal of fluorescein was noted. We evaluated the variation of the fluorescence intensity of fluorescein as a function of cesium ion concentration in the presence of PB nanoparticles. The results shown in Figure 10a,b indicate that the intensity of fluorescence did not depend on the cesium ion levels. The cesium–PB nanoparticle hybrid did not quench the fluorescence emission in a manner similar to that of As (III). The cesium ion concentration-dependent quenching of PB is shown in Figure 10c–g and justifies the sensing of cesium ions based on fluorescence quenching.

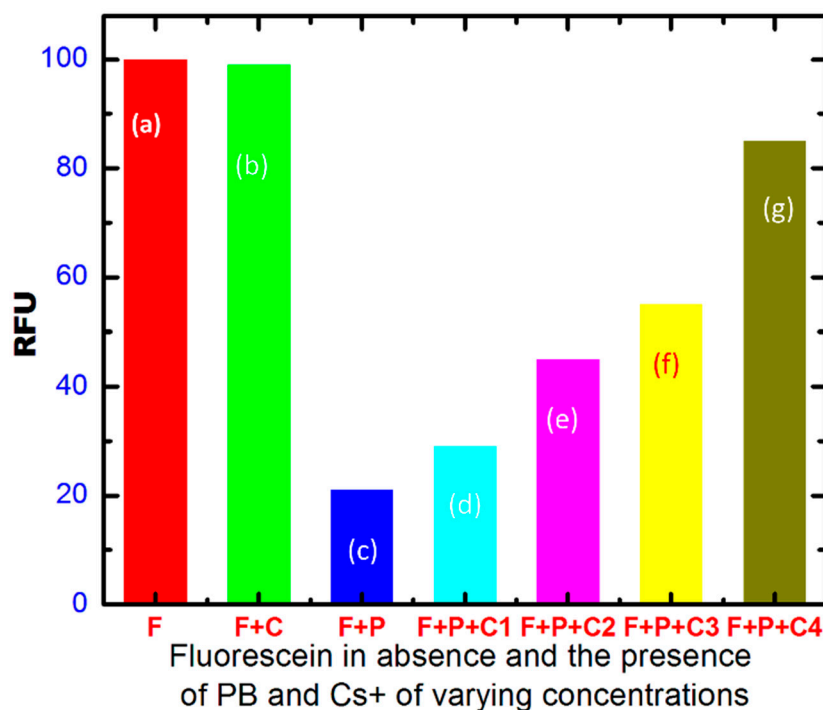


Figure 10. Fluorescence emission spectra of fluorescein. (a) Fluorescein and 200 ppm Cs⁺; (b) Fluorescein and PB nanoparticles; (c) Fluorescein containing PB and 50 ppm Cs⁺; (d) Fluorescein containing PB and 100 ppm Cs⁺; (e) Fluorescein containing PB and 300 ppm Cs⁺; (f) Fluorescein containing PB and 500 ppm Cs⁺; (g) Fluorescein containing PB and 1000 ppm Cs⁺.

4. Conclusions

PB nanoparticles were found to display analyte-dependent redox electrochemistry for selective sensing of hydrogen peroxide, arsenic (III), and cesium ions. The analyte-dependent intervalence transition between Fe³⁺ and Fe²⁺ in PB nanoparticles was for electrochemical sensing of As (III) and hydrogen peroxide based on differential pulse voltammetry. The opposite electrochemical interaction between As (III) and H₂O₂ with PB nanoparticles was recorded, indicating an analyte-dependent intervalence transition between the two iron centers. A peak energy corresponding to 2 eV associated with charge transfer reorganization energy between the two iron centers may be easily available during fluorescence emission, justifying the potent fluorescence quenching ability of PB nanoparticles. PB nanoparticle-mediated fluorescence sensing of the analyte, involving the intervalence transition between Fe³⁺ and Fe²⁺, was assessed. The PB nanoparticle-modified

SPE may serve as a cost-effective material for the removal of Cs⁺ from contaminated water, with (Q_{\max}) of Cs⁺ ions on the order of 325 mg·g⁻¹ in a 50 μM Cs⁺ solution, a distribution coefficient K_d on the order of 580 L·g⁻¹, and excellent reversibility for Cs⁺ removal.

Author Contributions: Conceptualization, P.C.P., validation, H.P.Y., Writing—original draft preparation, S.S.; writing—review and editing, P.C.P., R.J.N.; supervision, P.C.P., R.J.N. All authors have read and agreed to the published version of the manuscript.

Funding: The authors wish to knowledge SERB for Grant Number VJR-2017-000034 and DRDO for LSRB316 for support of this activity.

Institutional Review Board Statement: Not available.

Informed Consent Statement: Not available.

Data Availability Statement: All the data will be available to the readers.

Acknowledgments: The authors acknowledge support from SERB for the VAJRA Fellowship and DRDO for Grant LSRB-316.

Conflicts of Interest: The authors declare that they have no known competing financial interests or personal relationships that influence the work reported in this paper.

References

1. Vipin, A.K.; Fugetsu, B.; Sakata, I.; Isogai, A.; Endo, M.; Li, M.; Dresselhaus, M.S. Cellulose nanofiber backbone Prussian blue nanoparticles as powerful adsorbents for the selective elimination of radioactive cesium. *Sci. Rep.* **2016**, *6*, 37009. [CrossRef]
2. Yasunari, T.J.; Stohl, A.; Hayano, R.S.; Burkhart, J.F.; Eckhardt, S.; Yasunari, T. Cesium-137 deposition and contamination of Japanese soils due to the Fukushima nuclear accident. *Proc. Natl. Acad. Sci. USA* **2011**, *108*, 19530–19534. [CrossRef]
3. Hu, M.; Furukawa, S.; Ohtani, R.; Sukegawa, H.; Nemoto, Y.; Reboul, J.; Kitagawa, S.; Yamauchi, Y. Synthesis of Prussian blue nanoparticles with a hollow interior by controlled chemical etching. *Angew. Chem. Int. Ed.* **2012**, *51*, 984–988. [CrossRef]
4. Köhler, F.H.; Storcheva, O. Paramagnetic Prussian Blue Analogues CsMII [MIII (CN) 6]. The quest for spin on cesium ions by use of 133Cs MAS NMR spectroscopy. *Inorg. Chem.* **2015**, *54*, 6801–6806. [CrossRef]
5. Estelrich, J.; Busquets, M.A. Prussian blue: A safe pigment with zeolitic-like activity. *Int. J. Mol. Sci.* **2021**, *22*, 780. [CrossRef] [PubMed]
6. Faruque, H.A.; Choi, E.S.; Kim, J.H.; Kim, S.; Kim, E. In vivo removal of radioactive cesium compound using Prussian blue-deposited iron oxide nanoparticles. *Nanomedicine* **2019**, *14*, 3143–3158. [CrossRef]
7. Park, J.H.; Kim, H.; Kim, M.; Lim, J.M.; Ryu, J.; Kim, S. Sequential removal of radioactive Cs by electrochemical adsorption and desorption reaction using core-shell structured carbon nanofiber–Prussian blue composites. *Chem. Eng. J.* **2020**, *399*, 125817. [CrossRef]
8. Ohara, E.; Soejima, T.; Ito, S. Removal of low concentration Cs (I) from water using Prussian blue. *Inorg. Chim. Acta* **2021**, *514*, 120029. [CrossRef]
9. Chen, G.R.; Chang, Y.R.; Liu, X.; Kawamoto, T.; Tanaka, H.; Kitajima, A.; Parajuli, D.; Takasaki, M.; Yoshino, K.; Chen, M.L.; et al. Prussian blue (PB) granules for cesium (Cs) removal from drinking water. *Sep. Purif.* **2015**, *143*, 146–151. [CrossRef]
10. Kim, H.; Kim, M.; Lee, W.; Kim, S. Rapid removal of radioactive cesium by polyacrylonitrile nanofibers containing Prussian blue. *J. Hazard. Mater.* **2018**, *347*, 106–113. [CrossRef]
11. Rauwel, P.; Rauwel, E. Towards the extraction of radioactive cesium-137 from water via graphene/CNT and nanostructured Prussian blue hybrid nanocomposites: A review. *Nanomaterials* **2019**, *9*, 682. [CrossRef] [PubMed]
12. Pandey, P.C.; Pandey, A.K. Novel synthesis of super peroxidase mimetic polycrystalline mixed metal hexacyanoferrates nanoparticles dispersion. *Analyst* **2013**, *138*, 2295–2301. [CrossRef]
13. Pandey, P.C.; Pandey, A.K. Novel synthesis of Prussian blue nanoparticles and nanocomposite sol: Electro-analytical application in hydrogen peroxide sensing. *Electrochim. Acta* **2013**, *87*, 1–8. [CrossRef]
14. Pandey, P.C.; Pandey, A.K. A Process for the Polyethylenimine and Organic Reducing Agent-Mediated Synthesis of Noble Metal Nanoparticles. Indian Patent 295327, 6 January 2012.
15. Pandey, P.C.; Shukla, S.; Narayan, R.J. Organotrialkoxysilane-functionalized Prussian Blue nanoparticles-mediated fluorescence sensing of arsenic (III). *Nanomaterials* **2021**, *11*, 1145. [CrossRef]
16. Pandey, P.C.; Pandey, D. Tetrahydrofuran and hydrogen peroxide mediated conversion of potassium hexacyanoferrate into Prussian blue nanoparticles: Application to hydrogen peroxide sensing. *Electrochim. Acta* **2016**, *190*, 758–765. [CrossRef]
17. Rykov, A.I.; Wang, J.; Zhang, T.; Nomura, K. Cs sorption by “soluble” and “insoluble” iron hexacyanocobaltates probed by Mössbauer spectroscopy. *Hyperfine Interact.* **2013**, *218*, 53–58. [CrossRef]
18. Zheng, Y.; Qiao, J.; Yuan, J.; Shen, J.; Wang, A.J.; Niu, L. Electrochemical removal of radioactive cesium from nuclear waste using the dendritic copper hexacyanoferrate/carbon nanotube hybrids. *Electrochim. Acta* **2017**, *257*, 172–180. [CrossRef]

19. Murugappan, K.; Lee, J.; Silvester, D.S. Comparative study of screen printed electrodes for ammonia gas sensing in ionic liquids. *Electrochem. Commun.* **2011**, *13*, 1435–1438. [[CrossRef](#)]
20. O'Halloran, M.P.; Pravda, M.; Guilbault, G.G. Prussian Blue bulk modified screen-printed electrodes for H₂O₂ detection and for biosensors. *Talanta* **2001**, *55*, 605–611. [[CrossRef](#)]
21. Bonacin, J.A.; Santos, P.L.D.; Katik, V.; Foster, C.W.; Bank, C.E. Use of screen printed electrodes modified by Prussian blue and analogues in sensing of cysteine. *Electroanalysis* **2018**, *30*, 170–179. [[CrossRef](#)]
22. Cinti, S.; Arduini, E.; Moscone, D.; Palleschi, G.; Killard, A.J. Development of a hydrogen peroxide sensor based on screen-printed electrodes modified with inkjet-printed Prussian blue nanoparticles. *Sensors* **2014**, *14*, 14222–14234. [[CrossRef](#)]
23. Chen, R.; Tanaka, H.; Kawamoto, T.; Asai, M.; Fukushima, C.; Na, H.; Kurihara, M.; Watanabe, M.; Arisaka, M.; Nankawa, T. Selective removal of cesium ions from wastewater using copper hexacyanoferrate nanofilms in an electrochemical system. *Electrochim. Acta* **2013**, *87*, 119–125. [[CrossRef](#)]
24. Draouil, H.; Alvarez, L.; Causse, J.; Flaud, V.; Zaibi, M.A.; Bantignies, J.L.; Oueslati, M.; Cambedouzou, J. Copper hexacyanoferrate functionalized single-walled carbon nanotubes for selective cesium extraction. *New J. Chem.* **2017**, *41*, 7705–7713. [[CrossRef](#)]
25. Vipin, A.K.; Ling, S.; Fugetsu, B. Sodium cobalt hexacyanoferrate encapsulated in alginate vesicle with CNT for both cesium and strontium removal. *Carbohydr. Polym.* **2014**, *111*, 477–484. [[CrossRef](#)] [[PubMed](#)]
26. Yang, H.; Li, H.; Zhai, J.; Sun, L.; Zhao, Y.; Yu, H. Magnetic Prussian blue/graphene oxide nanocomposites caged in calcium alginate microbeads for elimination of cesium ions from water and soil. *Chem. Eng. J.* **2014**, *246*, 10–19. [[CrossRef](#)]
27. Yang, H.M.; Hwang, J.R.; Lee, D.Y.; Kim, K.B.; Park, C.W.; Kim, H.R.; Lee, K.W. Eco-friendly one-pot synthesis of Prussian blue-embedded magnetic hydrogel beads for the removal of cesium from water. *Sci. Rep.* **2018**, *8*, 11476. [[CrossRef](#)] [[PubMed](#)]
28. Li, T.; He, F.; Dai, Y. Prussian blue analog caged in chitosan surface-decorated carbon nanotubes for removal cesium and strontium. *J. Radioanal. Nucl. Chem.* **2016**, *310*, 1139–1145. [[CrossRef](#)]
29. Jang, S.C.; Haldorai, Y.; Lee, G.W.; Hwang, S.K.; Han, Y.K.; Roh, C.; Huh, Y.S. Porous three-dimensional graphene foam/Prussian blue composite for efficient removal of radioactive ¹³⁷Cs. *Sci. Rep.* **2015**, *5*, 17510. [[CrossRef](#)]